

Red-Edge Band Vegetation Indices for Leaf Area Index Estimation From Sentinel-2/MSI Imagery

Yuanheng Sun[✉], Qiming Qin, Huazhong Ren[✉], Tianyuan Zhang, and Shanshan Chen

Abstract—The estimation of leaf area index (LAI) from optical remotely sensed data based on vegetation indices (VIs) is a quick and practical approach to acquire LAI over vast areas. Reflectance in the red-edge bands is sensitive to vegetation status, and its information is thought to be useful in agricultural applications. Based on three red-edge band observations (represented as RE1, RE2, and RE3 for bands 5–7) from the Multispectral Instrument (MSI) onboard the Sentinel-2 satellite, this article aims to investigate the feasibility and performance of using red-edge bands for LAI estimates with the VI method and ground-measured LAI data sets. Sensitivity analysis from PROSAIL simulations revealed that RE1 is mainly affected by the influence of the leaf chlorophyll content, and this uncertainty should not be ignored during LAI estimation. For the normalized difference vegetation index (NDVI), modified simple ratio (MSR), chlorophyll index (CI), and wide dynamic range vegetation index (WDRVI), the optimal combination of Sentinel-2 bands for LAI estimation was RE2 and RE3, with a minimum root-mean-square error (RMSE) of 0.75. Four 3-band red-edge VIs were proposed to exploit the full content of the red-edge bands of Sentinel-2, and their performance in LAI estimation improved slightly. However, both 2-band red-edge VIs and 3-band red-edge VIs remained slightly saturated at high LAI levels; therefore, a segmental estimation with a threshold was suggested for large LAIs. The results indicate that the optimal 2-band red-edge VIs and proposed 3-band red-edge VIs are effective tools for crop LAI estimation in multiple-growth stages with Sentinel-2 MSI images.

Index Terms—Leaf area index (LAI), precision agriculture, red-edge, Sentinel-2, vegetation index.

I. INTRODUCTION

QUANTITATIVE retrieval of vegetation biophysical characteristics is an essential requirement in ecological and agricultural applications [1], [2], and one of these important variables is leaf area index (LAI), which describes the

Manuscript received June 24, 2019; revised August 6, 2019 and August 21, 2019; accepted August 28, 2019. This work was supported in part by the China National Major Project of High-Resolution Earth Observation under Grant 1-Y20A16-9001-17/18, in part by the Natural Science Foundation of China (NSFC) under Grant 41771371 and Grant 41771369, and in part by NSFC and Science and Technology Facilities Council (STFC) of UK Joint Program Project under Grant 61661136006002. (*Corresponding authors:* Qiming Qin; Huazhong Ren.)

The authors are with the Institute of Remote Sensing and Geographic Information System, Peking University, Beijing 100871, China, with the Beijing Key Laboratory of Spatial Information Integration and 3S Application, Peking University, Beijing 100871, China, and also with the Engineering Research Center for Geographical Information Basic Softwares and Applications, State Bureau of Surveying and Mapping, Beijing 100871, China (e-mail: yhsun@pku.edu.cn; qmqin@pku.edu.cn; renhuazhong@pku.edu.cn; zhangtianyuan@pku.edu.cn; shanshanchen@pku.edu.cn).

Color versions of one or more of the figures in this article are available online at <http://ieeexplore.ieee.org>.

Digital Object Identifier 10.1109/TGRS.2019.2940826

canopy structure of vegetation [3]. LAI is universally defined as the total one-sided area of photosynthetic tissue per unit ground area [4], [5], or half the total intercepting area per unit ground surface for nonflat leaves [6]. Based on the parts of vegetation that are accounted for, LAI can be divided into the plant area index (PAI) representing the green area, including the stem and wilted leaf and the purely green leaf area [7]. The green LAI or PAI is of great interest for agronomists and physiologists. In addition, different distributions of leaf foliage within a canopy can lead to different photosynthetic capacities, and the clumping index is used as an indicator to quantify the level of foliage grouping within distinct canopy structures [6]. Based on this concept, the true LAI multiplied by the clumping index is referred to as the effective LAI [8], [9]. To date, remote sensing has been the only feasible way to acquire LAI over a vast area, especially on the global scale [10]. In recent years, remote sensing-derived LAI has been extensively applied in crop growth monitoring [11], [12], agronomic management [13], [14], and yield estimation [15], [16] in agroecosystems. The knowledge of the spatial distribution of LAI allows farmers to be more precise in terms of fertilization and within-field water management [17].

The LAI retrieval methods from optical remote sensing data can be classified into three main categories: empirical, physically-based, and data-driven methods. Empirical models involve linear or nonlinear relationships between LAI and spectral reflectance or vegetation indices (VIs). This method is easy to implement, but it requires different calibrations with field measurements for particular vegetation types or areas [18], [19]. The physical-based method uses a radiative transfer model to simulate the motion of photons within the canopies and typically uses a look-up-table (LUT) strategy for retrieval [3], [7]. Compared to empirical methods, physically-based models are more accurate and applicable for a wider range of situations [20], but these models require more ancillary information per vegetation type for model parameterization, which is not always available. Data-driven models are a hybrid method that balance the advantages and weaknesses of the empirical and physically-based models and are constructed from massive simulated or *in situ* observation data sets using a machine learning approach [21]–[23]. However, the qualified data set for model training is not easy to obtain, and the training process may be fairly time-consuming.

The simple and computationally efficient empirical method remains of great interest for remote sensing LAI estimation. VIs are still the most extensive and effective variables for LAI estimation because they are dimensionless indicators

that can be used to depict the density or growth status of vegetation by using the contrast of spectral reflectance in different wavelengths, especially in the red and near-infrared (NIR) ranges. Among these indices, the normalized difference vegetation index (NDVI) is regarded as the most popular vegetation index for estimating vegetation biophysical characteristics [24]. However, the NDVI suffers from saturation at high LAI values, which is a limitation for its application in LAI retrieval [25]–[27]. To address this issue, Chen [28] evaluated several two-band VIs and proposed a modified simple ratio (MSR) index for LAI estimation in boreal forests. For crop LAI estimation, Gitelson [29] introduced a weighting coefficient to modify NDVI and consequently proposed the wide dynamic range vegetation index (WDRVI), whose sensitivity toward the moderate-to-high LAI values was claimed to be three times greater than that of the NDVI.

Apart from the conventional red and NIR bands, the potential of using the red-edge spectral information for LAI retrieval has also been demonstrated [30]–[32]. The red-edge of a vegetated spectrum is defined as the sharp change in the reflectance curve between 680 and 750 nm [33], and the shape of the red-edge region is strongly influenced by LAI because the canopy reflectance in the red-edge region mainly results from the multiple scattering between leaf layers [34], [35]. Meanwhile, there has been rapid technological progress over the last two decades in the development of moderate-to-high spatial resolution imaging sensors involving red-edge bands, including hyperspectral spectrometers such as Hyperion [30] and CHRIS [36], and multispectral sensors such as RapidEye [37] and WorldView-2 [38].

As an important component of the Copernicus program, Sentinel-2 satellites from the European Space Agency (ESA) provide imagery with three red-edge bands [39]. By exploiting the spectral information of red-edge bands from the Sentinel-2 configuration, some studies have demonstrated that the added red-edge spectral information can improve the accuracy of LAI [40], [41], chlorophyll content [42], [43] and biomass [44] estimations, while some other studies believed that the improvement in variable retrieval accuracy by using red-edge spectral information was not significant [45], [46].

Chlorophyll a and b content (hereafter called “chlorophyll content”) also has a great impact on the red-edge reflectance, and its increase can cause a shift in the red-edge position toward longer wavelengths [40], [47]. Thus, some red-edge VIs are also proposed to estimate the chlorophyll content [48], [49]. During the crop growth period, the canopy reflectance in red-edge and other bands varies simultaneously with the chlorophyll content and LAI changes, which makes the influence of the chlorophyll content nonnegligible for LAI estimation if the red-edge spectral indices are used. To address this issue, many studies have been carried out to explore the influence of red-edge spectral reflectance on LAI and chlorophyll content when red-edge spectral indices are used for parameter estimation based on the band configurations of some long-existing sensors, such as RapidEye [31], [50] and WorldView-2 [51]. Several recent works have focused on the individual influence of LAI and chlorophyll content on the reflectance of Sentinel-2 red-edge bands [43], [52];

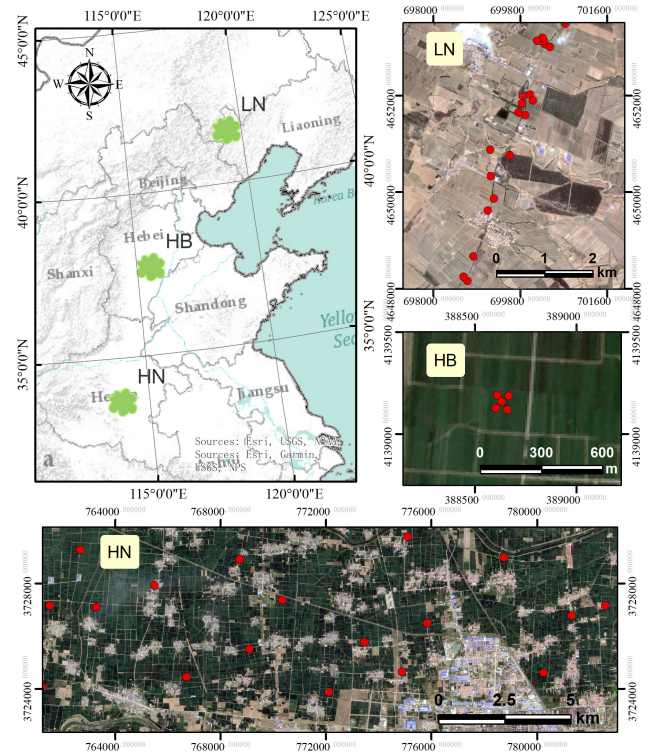


Fig. 1. Locations of the LN, HB, and HN experimental sites. The background images are the true color composite from Sentinel-2 collected on the dates corresponding to the fieldwork. Image coordinates (Northing and Easting) are in UTM Zone 50N projection based on a WGS-84 datum and spheroid.

however, the mutual influence of LAI and chlorophyll content on LAI has not been fully discussed. In addition, few studies have been conducted to determine whether using red-edge bands can improve the accuracy of LAI estimation with real Sentinel-2 imagery and *in situ* LAI observations; therefore, there remains some uncertainty of its usefulness.

This article tries to clarify the above issues with the following three research objectives: 1) analyze the individual and mutual influence of LAI and chlorophyll content on Sentinel-2 red-edge bands to find the optimal band for the LAI estimation; 2) check the performance of several classic VIs in LAI retrieval before and after using red-edge information based on Sentinel-2 imagery and *in situ* LAI measurements; and 3) evaluate several 3-band red-edge VIs that were proposed in this article for LAI retrieval.

II. GROUND-MEASURED LAI DATA AND SENTINEL-2 IMAGERY

A. Experimental Sites and *In Situ* LAI Collections

The field campaigns for LAI collection took place at three experimental sites located in Henan (HN), Hebei (HB), and Liaoning (LN) provinces, China (Fig. 1). The HN experimental site centered at 33.5° N, 114.1° E has a warm temperate monsoon (wet summer and dry winter) climate with a yearly average temperature of 14.6 °C and average precipitation of 805 mm. Winter wheat (*Triticum aestivum L.*) and maize (*Zea mays L.*) are the main crops in this region and are under rotation irrigated management practices. Wheat is sowed in

TABLE I
DATES OF FIELD MEASUREMENTS AND THE CORRESPONDING SENTINEL-2 IMAGES

Sites	Field Measurements Date	Sentinel-2 Image Date
Hebei	March 29, 2017 (winter wheat)	March 29, 2017
	May 4, 2017 (winter wheat)	April 28, 2017
	July 5, 2017 (maize)	July 7, 2017
	July 29, 2017 (maize)	August 3, 2017
Henan	March 8, 2018 (winter wheat)	March 9, 2018
	April 6, 2018 (winter wheat)	April 8, 2018
Liaoning	June 10, 2018 (maize)	June 11, 2018

early October and harvested in late May of the next year, while maize is cultivated from June to September. The HB experimental site has similar climate characteristics to that of HN, with central geographical coordinates of 37.5 N and 115.6 E. The annual average temperature of the HB site is approximately 12.7 °C, and average precipitation is approximately 510 mm. Wheat and maize are the dominant crops. The location of the LN experimental site is approximately 41.9 N, 119.4 E. The cultivated crop at the LN site is continuously irrigated maize. The crop is sowed in early May and harvested in October due to a relatively cold and more arid temperate monsoon climate with an annual temperature being 6.8 °C and precipitation of 480 mm.

LAI field measurements were carried out in these experimental sites from spring 2017 to summer 2018, covering the onset and peak of the crop growth cycle to maximize the dynamic range of the LAI data from different phenological states. Table I lists the dates of the measurements. At the HN experimental site, the LAI of winter wheat was measured on March 8, 2018 and April 6, 2018, from its tilling stage to the jointing stage. At the HB experimental site, the LAI of winter wheat was measured on March 29, 2017 and May 4, 2017, from its tilling stage to heading stage. At this site, the maize LAI was measured on July 5, 2017 and July 29, 2017, from its tilling stage to jointing stage. At the LN experimental site, the maize LAI was measured on June 10, 2018, under the tilling stage.

The above ground-based LAI was measured using an LAI-2000 Plant Canopy Analyzer (Li-Cor Inc., Lincoln, NE, USA). Since the crops are still in their vegetative stage and all the green parts of crops are detected during measurements, the measured total LAI can be understood as “effective green PAI” according to its definition introduced. For the HN experimental site, 32 elementary sampling units (ESUs) were established and evenly distributed across the homogeneous cropland region. Each ESU covered an area of approximately 5 m × 5 m, and five LAI measurements were collected; their average LAI was used to represent the final LAI value of the ESU. The same procedure was followed

TABLE II
SENTINEL-2 MSI BAND INFORMATION IN VNIR RANGE

Band	Central wavelength (nm)	Band width (nm)	Spatial resolution (m)
Coastal	443	20	60
Blue	490	65	10
Green	560	35	10
Red	665	30	10
RE1	705	15	20
RE2	740	15	20
RE3	783	20	20
NIR	842	115	10
NIR-A	865	20	20

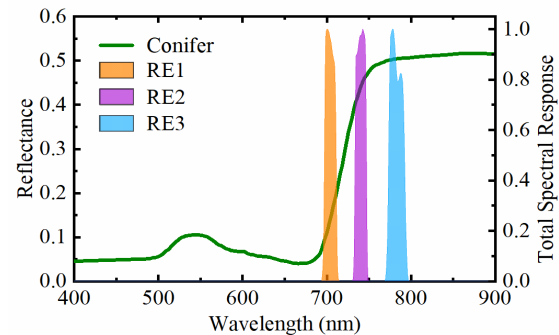


Fig. 2. Filters of three red-edge bands (RE1, RE2, and RE3) of Sentinel-2 with a typical conifer reflectance spectrum (source: USGS spectrum library).

for the HB and LN sites. The numbers of ESUs at the HB site and LN site were 55 and 24, respectively. All ESUs at the HB site were clustered into five LAI measurements in a homogeneous 100 m × 100 m area. The site layout is designed for future validation on LAI products at a much coarser spatial resolution. Nevertheless, a 5 m × 5 m ESU is our prime focus in this study. The distribution of the ESUs for *in situ* LAI observation is partly presented in Fig. 1 with their corresponding true color composite Sentinel-2 imagery as the background.

B. Sentinel-2/MSI Imageries Acquisition and Processing

The payload on the Sentinel-2 satellites, the Multispectral Instrument (MSI), comprises 13 bands including visible and near-infrared (VNIR, as shown in Table II) and shortwave infrared (SWIR) bands. Compared to other frequently-used multispectral sensors, such as Landsat-TM/ETM+/OLI and SPOT-HRV/HRG, Sentinel-2 has three additional red-edge bands located at 705, 740, and 783 nm (Fig. 2) in the VNIR domain with a spatial resolution of 20 m and a five-day revisit period when Sentinel-2A and Sentinel-2B data are combined under cloudless circumstances. It should be noted that RE3 of Sentinel-2 (band 7 centered at 783 nm) is out of the range where a sharp increase in reflectance occurs and quite close to the NIR domain (Fig. 2), so it is an NIR band more precisely. Since ESA has named it “red-edge band 3,” we still call it as RE3 in this article. The Sentinel-2 images used in this article are listed in Table I, and their dates are concurrent with those of the field campaign. These images

were downloaded from the Sentinels Scientific Data Hub (<http://scihub.copernicus.eu/>) as Level-1C orthorectified top of atmosphere (TOA) reflectance and then atmospherically corrected to obtain the top of canopy (TOC) reflectance using the Sen2Cor atmosphere correction toolbox (version 2.5.5) built in the Sentinel Application Platform (SNAP) software (version 6.0.0), which converted the TOA reflectance into the TOC reflectance [53]. The spatial resolutions of all bands were set to 20 m to guarantee the combined use of blue, red NIR, and red-edge bands.

III. NEW VEGETATION INDEXBASED METHOD FOR LAI ESTIMATION

To determine the influence of LAI and chlorophyll content on the band reflectance of Sentinel-2, simulated spectra under different LAIs and chlorophyll contents were first generated. Afterward, a sensitivity analysis was implemented to identify the significance of LAI and chlorophyll content to explain the variance in the Sentinel-2 band reflectance to develop a theoretical basis for optimal band selection for different VI forms. Next, the existing and improved VIs were introduced, and finally, we determined the optimal band combination and validated classic and newly proposed red-edge VIs against ground measurements.

A. Simulated Canopy Reflectance With PROSAIL Model

The canopy spectra were simulated using the PROSAIL model to check and analyze the influence of LAI and chlorophyll content (Cab) on the Sentinel-2 broad-band spectral reflectance, especially when they vary at the same time. The PROSAIL model, which couples the PROSPECT leaf optical properties model [54], [55] and Scattering by Arbitrarily Inclined Leaves (SAIL) canopy bidirectional reflectance model [56], [57], is widely used to model canopy spectra [58]. In this model, the canopy spectrum is mainly characterized by LAI, average leaf angle (ALA), leaf spectral reflectance and transmittance, which are a function of Cab, dry matter content (Cm), water content (Cw), leaf mesophyll structure index (N), and some other less influential factors.

As shown in Table III, the simulation sets LAI values from 1.0 to 8.0 with a step of 1.0 and chlorophyll content from 10 to 80 $\mu\text{g}/\text{cm}^2$ with a step of 5 $\mu\text{g}/\text{cm}^2$. The grayish-brown loam that is widespread in northern China was selected as the background soil for the PROSAIL model, and its spectrum was obtained from the Johns Hopkins University (JHU) spectra database [59]. Other parameters of the PROSAIL model were assigned a fixed value based on our field measurements and related literature [60] for wheat and maize, as listed in Table III. Finally, the simulated canopy spectral reflectance was integrated into the band reflectance using the Sentinel-2/MSI spectral filters.

B. Sensitivity Analysis Methods for Sentinel-2 Red-Edge Bands

Both local and global sensitivity analyses were implemented to quantify the significance of LAI and chlorophyll content

TABLE III
NOMINAL VALUES OR RANGES OF PARAMETERS USED IN THE PROSAIL MODEL

Input parameter	value or range
<i>Cab</i> (chlorophyll content, $\mu\text{g}/\text{cm}^2$)	10–80, step: 5
<i>Car</i> (carotenoids content, $\mu\text{g}/\text{cm}^2$)	$0.2 \times \text{Cab}$
<i>Cw</i> (water content, g/cm^2)	0.01
<i>Cm</i> (dry matter content, g/cm^2)	0.005
<i>N</i> (leaf mesophyll structure index)	1.5
<i>LAI</i> (leaf area index, m^2/m^2)	1~8, step: 1
<i>ALA</i> (average leaf angle, $^\circ$)	57
θ_s (solar zenith angle, $^\circ$)	30
θ_v (view zenith angle, $^\circ$)	0
ϕ (relative azimuth angle, $^\circ$)	0

in explaining the variance in the canopy reflectance. The reflectance of the three red-edge Sentinel-2 bands (B5, centered at 705 nm, represented as RE1; B6, centered at 740 nm, represented as RE2; and B7, centered at 783 nm, represented as RE3), together with red (B4, centered at 665 nm) and NIR bands (B8, centered at 842 nm), were investigated to determine whether and to what extent the variation in LAI and chlorophyll content impacted them.

For the local sensitivity analysis, LAI was fixed at different levels, and ΔRef was calculated as an indicator to quantify the relative change in band reflectance between two different chlorophyll contents

$$\Delta\text{Ref} = \left| \frac{\text{Ref}_2 - \text{Ref}_1}{\text{Ref}_1} \times 100\% \right| \quad (1)$$

where Ref_1 is the band reflectance of the red, red-edge, or NIR band of Sentinel-2 under one chlorophyll content, referred to as the reference reflectance in (1), while Ref_2 is the corresponding reflectance under another chlorophyll content.

The influence of a single parameter on the outcome is rarely completely independent. Coupling interactions usually exist between various parameters but are not taken into account in local sensitivity analysis methods [61]. Thus, the extended Fourier amplitude sensitivity test (EFAST) approach which is capable of describing the coupling interactions was adopted in this study. This variance-based method performs a judicious deterministic sampling to explore the parameter space, allowing for the reduction of these integrals to 1-D integrals using Fourier decompositions [62], [63]. It allows the estimation of firstorder (individual) and total (joint) Sobol indices for all the factors contributing to the canopy spectrum in the PROSAIL model with high computational efficiency. In this practice, the calculation by EFAST is limited to sensitivities referring to the main effect (additive influence of individual input factor) and total effect (an overall measurement of the contribution of a factor coupling with others). Taking a particular factor LAI for instance, its main effect gives the influence of LAI independently, while the total effect is the joint contribution of LAI with other factors. In other words, the difference between the main effect and the total effect of LAI is the effect of its interaction with others. On the basis of the above PROSAIL simulated data set this article conducted a global

TABLE IV
POTENTIAL VIs FOR SENTINEL-2 LAI ESTIMATION

Index	Formula	References
NDVI	$\frac{R_{\text{nir}} - R_{\text{red}}}{R_{\text{nir}} + R_{\text{red}}}$	[24]
MSR	$\frac{(R_{\text{nir}}/R_{\text{red}}) - 1}{\sqrt{(R_{\text{nir}}/R_{\text{red}}) + 1}}$	[28]
red-edge CI	$\frac{R_{\text{nir}} - 1}{R_{\text{re}}}$	[48], [49]
green CI	$\frac{R_{\text{nir}} - 1}{R_{\text{green}}}$	[48], [49]
WDRVI	$\frac{c * R_{\text{nir}} - R_{\text{red}}}{c * R_{\text{nir}} + R_{\text{red}}} + \frac{1 - c}{1 + c}$	[29], [67]

*The subscript *re* stands for red-edge. *c* is coefficient and the default value is set to 0.1.

analysis with the EFAST method with the Sensitivity Package (version 1.15.2) on the R platform (version 3.5.1).

C. Existing and Improved Vegetation Indices

VIs were derived from the surface reflectance of Sentinel-2 imageries for subsequent LAI retrieval. Some of the potential VIs used for Sentinel-2 LAI estimation are listed in Table IV. NDVI is an effective and widely used VI benchmark with an inherent drawback of saturation under moderate-to-dense canopies. VIs such as MSR and WDRVI are also based on red and NIR band reflectance. Chlorophyll-related VIs such as the red-edge chlorophyll index (CI) also exhibit a linear relationship with LAI [64], which can reduce the abovementioned saturation issue of NDVI to a certain extent. As such, the red-edge located in the wavelength range from red to NIR with rapid reflectance increases has the potential to replace red or even NIR reflectance in the NDVI, MSR, WDRVI and red-edge CI for constructing novel indices to suppress the saturation problem in the current VIs [65], [66]. Original red-edge CI will be referred to as CI for short afterward.

Different band combinations among red, red-edge and NIR of Sentinel-2 were tested for NDVI, MSR, CI and WDRVI (Table IV) to determine the optimal combination for LAI estimation. The introduction of red-edge bands in VIs can improve the performance in LAI estimation [48], [49], [65], but the VIs mentioned above only use one red-edge band. To make full use of the red-edge band information, we combine three red-edge bands for Sentinel-2 LAI retrieval. As a result four new VIs that exploit the spectral information of all three red-edge bands were proposed: 3-band red-edge NDVI (3NDVI_{re}), 3-band red-edge MSR (3MSR_{re}), 3-band red-edge CI (3CI_{re}) and 3-band red-edge WDRVI ($3\text{WDRVI}_{\text{re}}$). The four VIs are calculated as the weighted average of two conventional 2-band VIs with different red-edge bands as shown in (2)–(5). The subscripts *re1*, *re2* and *re3* corresponded to the three red-edge bands (RE1, RE2 and RE3 in Table II)

$$3\text{NDVI}_{\text{re}} = a \frac{R_{\text{re}3} - R_{\text{re}1}}{R_{\text{re}3} + R_{\text{re}1}} + (1 - a) \frac{R_{\text{re}3} - R_{\text{re}2}}{R_{\text{re}3} + R_{\text{re}2}} \quad (2)$$

$$3\text{MSR}_{\text{re}} = a \frac{(R_{\text{re}3}/R_{\text{re}1}) - 1}{\sqrt{(R_{\text{re}3}/R_{\text{re}1}) + 1}} + (1 - a) \frac{(R_{\text{re}3}/R_{\text{re}2}) - 1}{\sqrt{(R_{\text{re}3}/R_{\text{re}2}) + 1}} \quad (3)$$

$$3\text{CI}_{\text{re}} = a \left(\frac{R_{\text{re}3}}{R_{\text{re}1}} - 1 \right) + (1 - a) \left(\frac{R_{\text{re}3}}{R_{\text{re}2}} - 1 \right) \quad (4)$$

$$3\text{WDRVI}_{\text{re}} = a \left(\frac{c * R_{\text{re}3} - R_{\text{re}1}}{c * R_{\text{re}3} + R_{\text{re}1}} + \frac{1 - c}{1 + c} \right) + (1 - a) \left(\frac{c * R_{\text{re}3} - R_{\text{re}2}}{c * R_{\text{re}3} + R_{\text{re}2}} + \frac{1 - c}{1 + c} \right). \quad (5)$$

The use of red-edge spectral information could eliminate the saturation problem but it could also lead to sensitivity to chlorophyll content. Thus the weighted coefficient “*a*” in the equations is designed to balance the decrease in the degree of saturation and the influence of the chlorophyll content. This coefficient is band-dependent and is determined by *in situ* LAI observations and the corresponding VIs derived from Sentinel-2 in Section III-D

D. Comparison and Validation Methods for Different Vegetation Indices

The performance of the VIs discussed in Section III-C in LAI estimation was evaluated with a *k*-fold cross-validation procedure by using *in situ* observations and their corresponding Sentinel-2 data [68]. The entire LAI data set obtained from the LN, HB, and HN experimental sites was randomly divided into *k* mutually exclusive equal-size groups. In the *k* groups, *k* – 1 groups were selected as the training data set, while the rest were used as the validation data set. This process was repeated *k* times to ensure that each group could be used as validation and the rest were used as the training data set. This kind of validation method avoids the dependence on a single random partition into validation data sets and guarantees that all samples are used for both training and validation with the same probability. In this case, we used a tenfold (*k* = 10) cross-validation procedure. Finally, the coefficient of determination (R^2) of the VIs and the corresponding measured LAI and the root-mean-square error (RMSE) of the estimated LAI and measured LAI were selected as the indicators to evaluate the performance of these VIs.

IV. RESULTS

A. Spectral Characteristics of Sentinel-2 Red-Edge Bands

Fig. 3 demonstrates the variation of the relative difference in reflectance with chlorophyll contents of 20 and 70 $\mu\text{g}/\text{cm}^2$ under different LAI values. The red, RE1, RE2, and RE3, and NIR correspond to the Sentinel-2 MSI bands 4–8 configurations, respectively. RE1 has the largest variation in the reflectance ratio, and ΔRE1 increases as LAI increases and it reaches 35% when LAI = 8, which indicates that the RE1 band is significantly affected by the chlorophyll content. The values for ΔRE2 and ΔRE3 are lower than ΔRE1 but steadily increase as LAI increases. For example, ΔRE2 and ΔRE3 increase by 9.4% and 3.9%, respectively, as the chlorophyll content varies from 20 to 70 $\mu\text{g}/\text{cm}^2$ for LAI = 3 (median vegetation). However, these values only

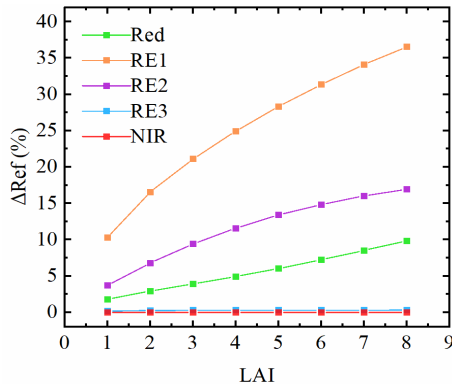


Fig. 3. Relative changes in band reflectance (ΔRef) under different LAI values, with chlorophyll content changing from 20 and $70 \mu\text{g}/\text{cm}^2$.

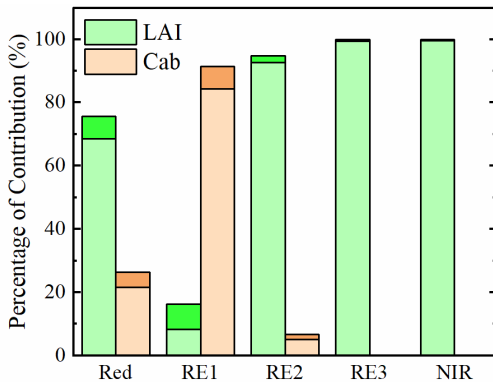


Fig. 4. Main effect and interaction of sensitivity analysis on LAI and chlorophyll content on Sentinel-2 band reflectance. The light color represents the main effect (independent contribution), and the dark color represents the interaction.

increase to 14.8% and 7.3% for the samples of $\text{LAI} = 6$ (dense vegetation). For the RE3 and NIR bands, their relative changes in the reflectance at different chlorophyll contents are nearly 0.0 in all LAI ranges, indicating that the chlorophyll content has nearly no impact on these two bands.

The sensitivity outcome on chlorophyll content might be diverse under different LAI values due to interactions between the effect of chlorophyll content and LAI, and vice versa. Therefore apart from individual sensitivity analysis of the chlorophyll content and LAI, the EFAST global sensitivity analysis method was introduced to reveal the mutual effect of the LAI, chlorophyll content and other parameters on the reflectance of Sentinel-2 red-edge bands. Fig. 4 presents the main effect and interaction of the contribution of LAI and chlorophyll content on the reflectance. In the red band the sum of the main effect of LAI and chlorophyll content is 90% (68.5% for LAI and 21.5% for chlorophyll content), which means that approximately 90% of the information on the red band reflectance from the PROSAIL model can be explained by LAI and chlorophyll content, and the remaining 10% can be explained by the interactions with other parameters. For the RE1 band, the chlorophyll content contributes most to the band reflectance information, with the main effect of 84.4% and an interaction of 7.1% while the LAI only contributes 8.3%. For

TABLE V
DETERMINATION COEFFICIENT (R^2) OF LINEAR REGRESSION FOR DIFFERENT BAND COMBINATIONS OF SENTINEL-2 VNIR IN NDVI-LIKE, MSR-LIKE, CI-LIKE, AND WDRVI-LIKE VIs

Band combination of Sentinel-2	NDVI	MSR	CI	WDRVI
Red, NIR	0.7072	0.8170	0.7835	0.7987
RE1, NIR	0.7430	0.8149	0.8301	0.8134
RE2, NIR	0.8128	0.8162	0.8178	0.8173
Red, RE3	0.7107	0.8243	0.7916	0.8055
RE1, RE3	0.7492	0.8255	0.8428	0.8246
RE2, RE3	0.8450	0.8492	0.8513	0.8506
Red, RE2	0.7196	0.7960	0.7672	0.7906
RE1, RE2	0.7427	0.7891	0.8034	0.7933
Green, NIR	-	-	0.8166	-
Green, RE3	-	-	0.8266	-
Green, RE2	-	-	0.7847	-

the RE2 band, the LAI accounts for 92.8% of the information in the reflectance with fewer interactions, and the chlorophyll content explains only 5.1%. Finally, almost all the information in the RE3 and NIR bands comes from the influence of the LAI which is in agreement with the local sensitivity analysis results in Fig. 3.

The impact of the chlorophyll content on the three red-edge bands of the Sentinel-2 MSI configuration decreases sharply toward longer wavelengths with the main effects of 84.4%, 5.1% and nearly 0.0% for RE1, RE2 and RE3 respectively. The influence of the chlorophyll content on the red band is greater than that of RE2 and RE3 but much lower than that of RE1 based on the global analysis results. In the local sensitivity analysis (see Fig. 3), ΔRE2 is larger than ΔRed when the chlorophyll content varies from 20 to $70 \mu\text{g}/\text{cm}^2$ but still far less than ΔRE1 . Based on these results, it can be concluded that the RE1 of Sentinel-2 is severely affected by the chlorophyll content, whereas the red and RE2 are moderately influenced and RE3 and NIR are minimally influenced.

B. Optimal Relationship Between VIs and LAI

Among the three red-edge bands, it is necessary to determine the optimal red-edge band as well as the vegetation index for LAI estimation. Table V provides the determination coefficient (R^2) for the linear regression which can reflect the saturation effect, between *in situ* LAI observations and NDVI-like, MSR-like, CI-like and WDRVI-like VIs using different combinations of Sentinel-2 bands. It was found that the combination of bands RE2 and RE3 in the four VIs results in the strongest correlations with LAI. The formulas of these VIs with optimal bands of Sentinel-2 are shown in (6)–(9). The combination of RE1 and RE3 is observed as the second largest R^2 . Although a strong correlation with LAI is observed, the RE1 VIs are still not good options due to their sensitivity to the chlorophyll content as discussed in Section IV-A, and its value is still needed to be tested. For the NDVI-like indices saturation also occurs when red and RE1 are used. With the introduction of RE2 and RE3 to replace red and NIR, such saturation is reduced to a great extent allowing the R^2 to increase from 0.7072 (row 2 of Table V) to 0.8450 (row 6).

The other forms of VIs have an acceptable performance with the conventional red and NIR in the calculation, and the replacement of red-edge bands only slightly improves their correlation with ground-measured LAI. Green CI was calculated as the ratio of NIR and green when it was initially proposed; thus, it works better with green than red but slightly worse than RE1 or RE2

$$\text{NDVI}_{\text{re}} = \frac{R_{\text{re}3} - R_{\text{re}2}}{R_{\text{re}3} + R_{\text{re}2}} \quad (6)$$

$$\text{MSR}_{\text{re}} = \frac{(R_{\text{re}3}/R_{\text{re}2}) - 1}{\sqrt{(R_{\text{re}3}/R_{\text{re}2}) + 1}} \quad (7)$$

$$\text{CI}_{\text{re}} = \frac{R_{\text{re}3}}{R_{\text{re}2}} - 1 \quad (8)$$

$$\text{WDRVI}_{\text{re}} = \frac{c * R_{\text{re}3} - R_{\text{re}2}}{c * R_{\text{re}3} + R_{\text{re}2}} + \frac{1 - c}{1 + c}. \quad (9)$$

The scatterplots of *in situ* LAI and VIs based on red and NIR are presented in the left column of Fig. 5. For CI, the RE1 is used in its calculation. The NDVI exhibits an exponential relationship with LAI but is saturated after LAI exceeds 3. The MSR and WDRVI overcome the saturation problem to a certain extent, as does the CI when using the band RE1. The use of RE2 and RE3 increases the correlation between LAI and VIs (Fig. 5 right column). The employment of the red-edge band can improve the performance of NDVI when there is saturation [see Fig. 5(b)] and slightly enhances the performance of the other three VIs. However, the use of red-edge bands cannot completely remove the saturation effect and saturation could be still observed for large LAIs (e.g., LAI > 4) for all these indices. The uncertainty of ground measured LAI data in the dense vegetated condition is higher than that of the sparse-to-moderate vegetation. Therefore more reliable *in situ* LAI data are needed to explore the performance of these indices, and the saturation problem remains an issue that needs to be improved further.

The 3-band red-edge VIs in (2)–(5) were calculated using the Sentinel-2 reflectance data with the parameter “ a ” varying from 0.0 to 1.0 with a step of 0.1. The parameter “ a ” represents the proportion of the VIs using RE3 and RE1, and the parameter “ $(1 - a)$ ” represents the proportion of the VIs using RE3 and RE2. The determination coefficients (R^2) of different 3-band red-edge VIs and LAI in the linear regression model under a series of “ a ” values are shown in Fig. 6. All these indices perform similarly at $a = 0$ (meaning only RE3 and RE2 are used), but their performance diverges with the added information of RE1. The curve of the 3-band red-edge vegetation index based on NDVI (3NDVI_{re}) follows a monotone decreasing pattern, with the greatest R^2 at $a = 0$, and its R^2 is far smaller than that of the other three indices as a approaches 1. The R^2 of 3MSR_{re}, 3CI_{re} and 3WDRVI_{re} peak at $a = 0.1$ and their curves show the same trend: a slight increase from $a = 0.0$ to $a = 0.1$, and then a decrease until $a = 1.0$. The 3CI_{re} has the best performance compared to 3MSR_{re} and 3WDRVI_{re} while the remaining two indices perform very similar. All the 3-band red-edge VIs proposed obtained a higher R^2 when $a = 0.0$ compared to when $a = 1.0$, suggesting that using RE2 information results in a better performance in LAI estimation as opposed to

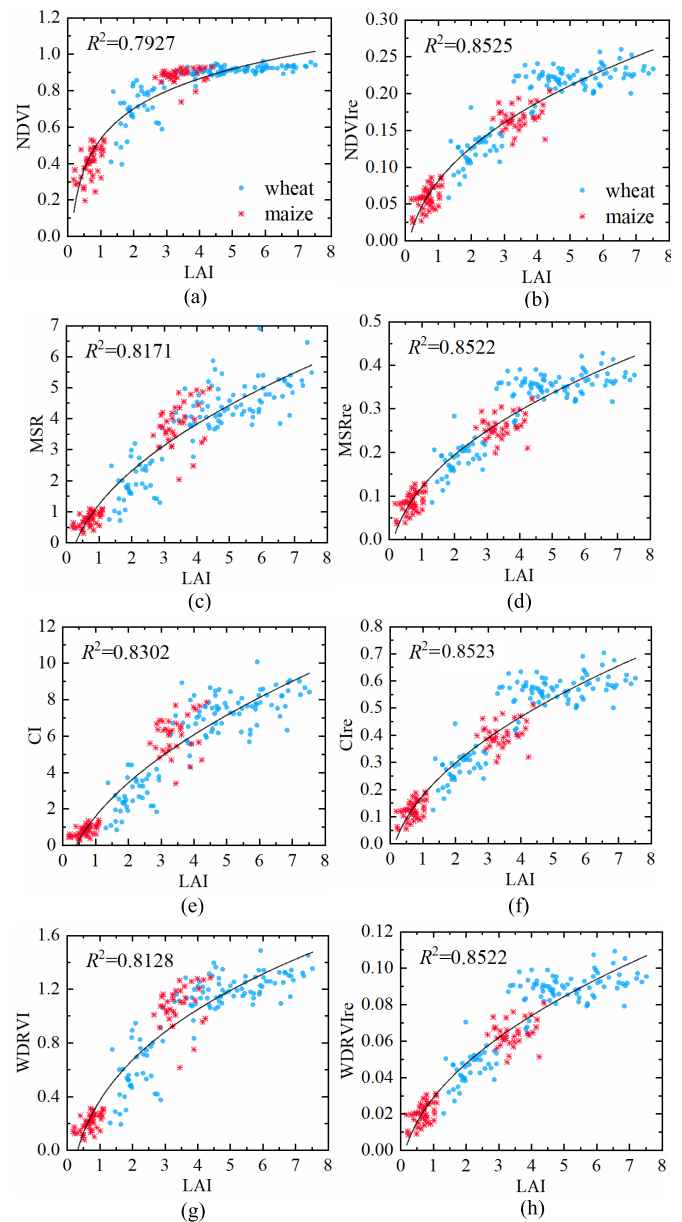


Fig. 5. Relationships between ground-measured LAI and VIs (NDVI, NDVI_{re}, MSR, MSRe, CI, Cire, WDRVI, and WDRVIRE) derived from Sentinel-2 imageries of the experimental sites. (a) LAI and NDVI. (b) LAI and NDVI_{re}. (c) LAI and MSR. (d) LAI and MSRe. (e) LAI and CI. (f) LAI and Cire. (g) LAI and WDRVI. (h) LAI and WDRVIRE.

using RE1 information. Therefore, combining the information of the three red-edge band reflectance of Sentinel-2 with an appropriate proportion (i.e. $a = 0.1$ in our case) will further improve the correlation between LAI and the VIs. However, given the variation in crop types and the other factors of the agricultural system a should be updated in accordance with more factors before being applied in a new region.

C. Validation for VI Based LAI Estimation Models

The results of the tenfold cross-validation for LAI estimation on different VIs are presented in Figs. 7–9, and the best-fit regression algorithms of each vegetation index for the ground-measured LAI of wheat and maize are presented in Table VI.

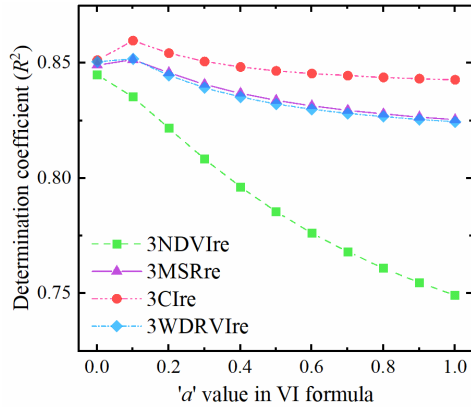


Fig. 6. Determination coefficients (R^2) of the linear regression from 3-band red-edge VIs to LAI under different values of the parameter a .

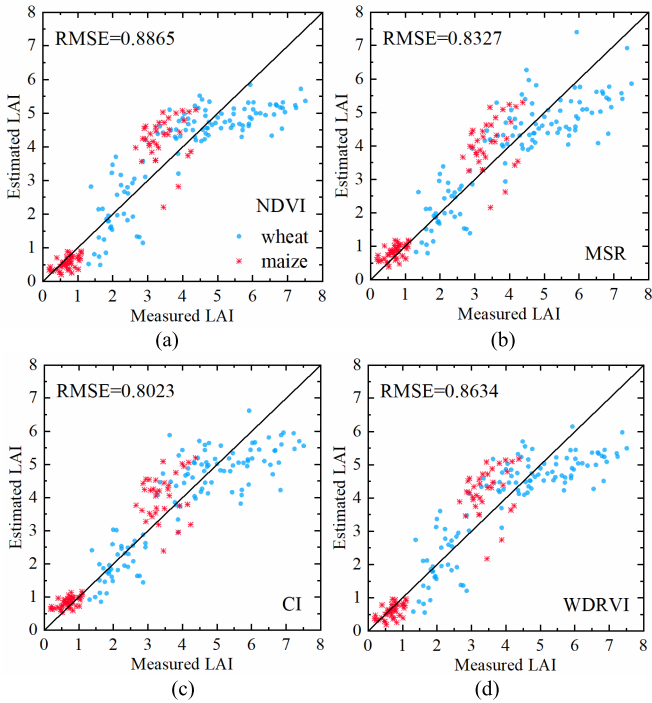


Fig. 7. Ground-measured LAI and estimated LAI from (a) NDVI-, (b) MSR-, (c) CI-, and (d) WDRVI-based methods.

The R^2 and RMSE were selected as the indicators to evaluate their performance. The NDVI-based model performs the worst [Fig. 7(a)], and a significant underestimation is observed at large LAIs, illustrating that VIs are not a good option. The WDRVI [Fig. 7(d)] still has a problem of saturation and results in an estimation similar to that of the NDVI. The other two VIs, MSR and CI [Fig. 7(b) and (c)], show better LAI estimation power, and the RMSE of the LAI estimated using these two indices decreases to 0.83 and 0.80. With the optimal band combination of RE2 and RE3, the performance of the NDVIre-based model [Fig. 8(a)] improves the LAI estimate accuracy significantly compared to the conventional NDVI-based model, with RMSE decreasing from 0.89 to 0.75. Meanwhile, the improvements in MSRe, CIre, and WDRVIre are not as prominent compared to the improvement in NDVIre, as shown in Fig. 8(b)–(d). However, the most prominent

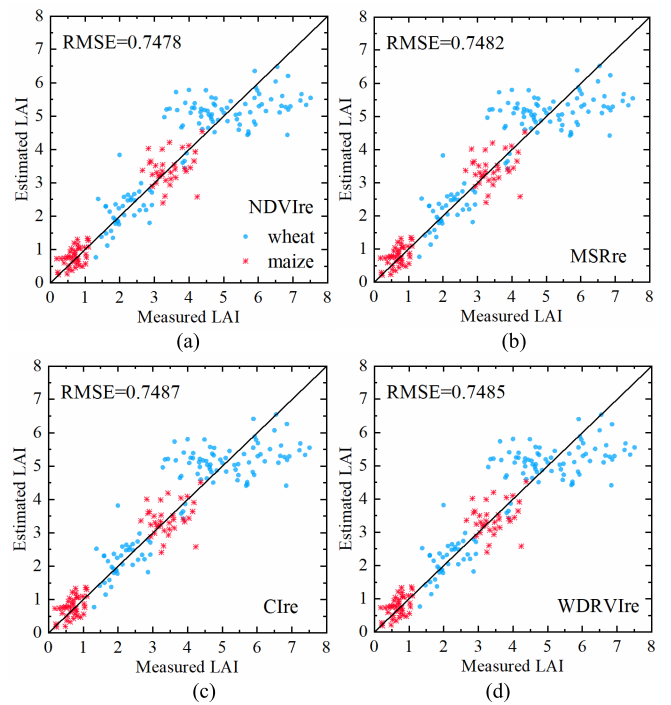


Fig. 8. Ground-measured LAI and estimated LAI from (a) NDVIre-, (b) MSRe-, (c) CIre-, and (d) WDRVIre-based methods.

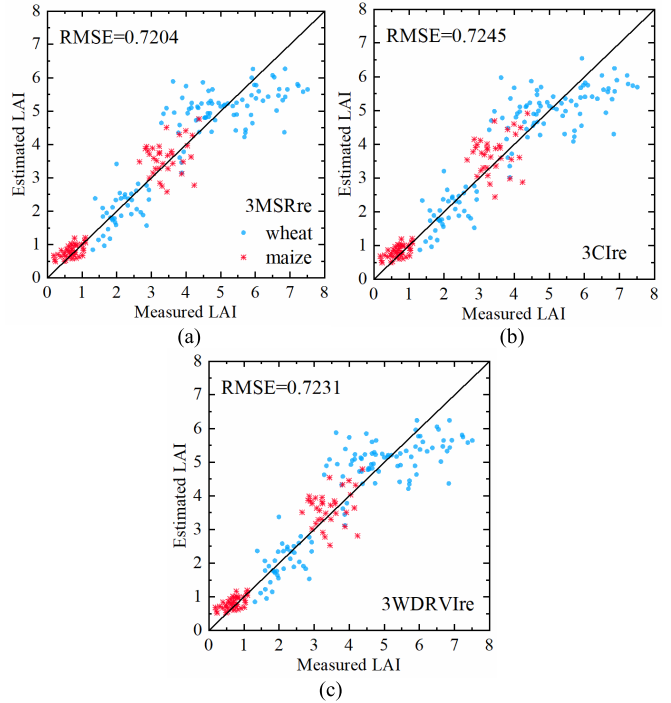


Fig. 9. Ground-measured LAI and estimated LAI from (a) 3MSRre-, (b) 3CIre-, and (c) 3WDRVre-based methods.

contribution of the red-edge VIs in LAI estimation is their suppression of the overestimation of LAI in moderate-vegetated conditions both for wheat and maize. The scatterplots of moderate LAI estimation results ($2 < \text{LAI} < 5$) are mainly above the 1:1 lines (Fig. 8), while the scatterplots for the

TABLE VI
BEST-FIT UNIFIED ALGORITHMS FOR THE WHEAT AND MAIZE DATA SETS BASED ON THE ORIGINAL VIs,
2-BAND RED-EDGE VIs, AND PROPOSED 3-BAND RED-EDGE VIs FOR LAI ESTIMATION

	Vegetation index	$\text{LAI} = f(\text{VI})$	R^2	RMSE
Original VIs	NDVI	$0.0875e^{4.372x}$	0.79	0.887
	MSR	$0.091 + 0.9898x^{1.035}$	0.82	0.833
	CI	$0.3808 + 0.5613x^{1.0426}$	0.83	0.802
	WDRVI	$3.8459x^{1.1808}$	0.81	0.863
2-band red-edge VIs	NDVIRE	$0.0328 + 46.0712x^{1.4608}$	0.85	0.749
	MSRRE	$-0.0771 + 19.4947x^{1.2759}$	0.85	0.748
	CIRE	$-0.1855 + 10.0192x^{1.1272}$	0.85	0.749
	WDRVIRE	$-0.135 + 92.7165x^{1.1887}$	0.85	0.749
3-band red-edge VIs	3MSRRE	$0.3715 + 12.0831x^{1.5927}$	0.86	0.720
	3CIRE	$0.3116 + 3.7334x^{1.1915}$	0.86	0.725
	3WDRVIRE	$0.4229 + 85.952x^{1.5444}$	0.86	0.723

NDVIRE, MSRRE, CIRE, and WDRVIRE are closer to 1:1 lines (Fig. 8).

The results of the proposed 3-band red-edge VIs [3MSRRE, 3CIRE, and 3WDRVIRE, in (3)–(5)] with an optimal “ a ” value (0.1 in our case) are presented in Fig. 9. Since the optimal a value of 3NDVIRE is 0.0 (see Fig. 6), its result is equivalent to that of NDVIRE in Fig. 8(a) and thus not included here. Compared to the 2-band red-edge VIs, the 3-band models achieve similar performance in sparsely-vegetated conditions (i.e., $\text{LAI} < 2$) and in moderate-to-dense-vegetated conditions (i.e., $2 < \text{LAI} < 5$). The overall RMSEs of the 3MSRRE, 3CIRE, and 3WDRVIRE-based methods are 0.720, 0.725, and 0.723, respectively, which are slightly lower than the 2-band red-edge vegetation index-based methods.

The above ground validation shows that the inclusion of red-edge bands in VIs is generally reasonable. The results provide evidence from satellite reflectance and ground-measured data that the use of RE2 and RE3 can improve the LAI estimate mainly because the two bands are less influenced by the chlorophyll content than the red and RE1 bands. These 3-band red-edge VIs (3MSRRE, 3CIRE and 3WDRVIRE) achieve the highest LAI estimation accuracy and thus are recommended for LAI estimation. However, if there is a lack of prior knowledge on the update of parameter “ a ” in these VIs before being applied in a new region, the optimal 2-band red-edge VIs (NDVIRE, MSRRE, CIRE and WDRVIRE) should be considered first for their robustness. The original VIs (NDVI, MSR, CI and WDRVI) are suitable for sparse-to-moderately vegetated conditions if the LAI mapping requires high spatial resolution (e.g., 10 m).

D. LAI Image Retrieval Using Red-Edge Vegetation Index-Based Method

The wheat-cultivated region near the HB experimental site is chosen to illustrate the LAI image estimated from red-edge VIs during the growing season of 2017. The dates of the presented LAI images, March 29 and April 28, correspond to moderate and dense crop conditions, respectively.

The LAI images of nonvegetated areas extracted on March 29 are presented in Figs. 10 and 11, and the LAI results derived from the original VIs are also illustrated for

comparison. The NDVI-based method results in more pixels in the LAI value subrange [0, 1], while more pixels are in the LAI value subrange [2, 4] for the NDVIRE-based result [Fig. 10(c)]. Pixels with high LAI values can be observed in the bottom-right corner of the NDVI-based LAI image [Fig. 10(a)], which is not reasonable during the winter wheat growth period. This unreasonable result is also manifested in the histograms in Fig. 10(c). Thus, the NDVI-based result may not be reliable in this specific region and period. Except for the NDVI- and NDVIRE-based methods, the families of MSR (MSR, MSRRE, and 3MSRRE) are also chosen to generate LAI images with their best-fit regression method (see Table VI). All of them are shown to have achieved similar LAI images and LAI histograms, and the two results involving red-edge bands (MSRRE-based and 3MSRRE-based) are slightly higher than the MSR-based LAI result (Fig. 11).

The LAI images with nonvegetated areas extracted on April 28 are presented in Figs. 12 and 13. Few pixels exhibit an LAI value higher than 5.5 when using the NDVI-based approach, clearly demonstrating its saturation problem in LAI estimation under densely-vegetated conditions [Fig. 12(c)]. In contrast, the result from the NDVIRE-based method shows more pixels in the LAI value subrange [5.5, 7]. The MSR-based method results in more pixels in the LAI value subrange [5.5, 7] compared to the NDVI-based result, which is in accordance with the previous findings in Section IV-B that explain how MSR could overcome the saturation issue to a certain extent [28]. However, pixels with extremely high LAI values appear in their LAI image, thus proving that this method is not robust enough to employ in dense crop monitoring. After the introduction of red-edge bands, the number of pixels in the LAI value subrange [5.5, 7] from MSRRE- and 3MSRRE-based methods increases compared to the MSR-based result (Fig. 13), and their performance is fairly similar.

V. DISCUSSION

Quantitative determination and mapping of LAI using medium-resolution optical imagery is always a challenging task especially for dense canopies [69], [70]. Many studies have shown variation and uncertainty between LAI and VIs due to the tendency for spectral indices to become saturated

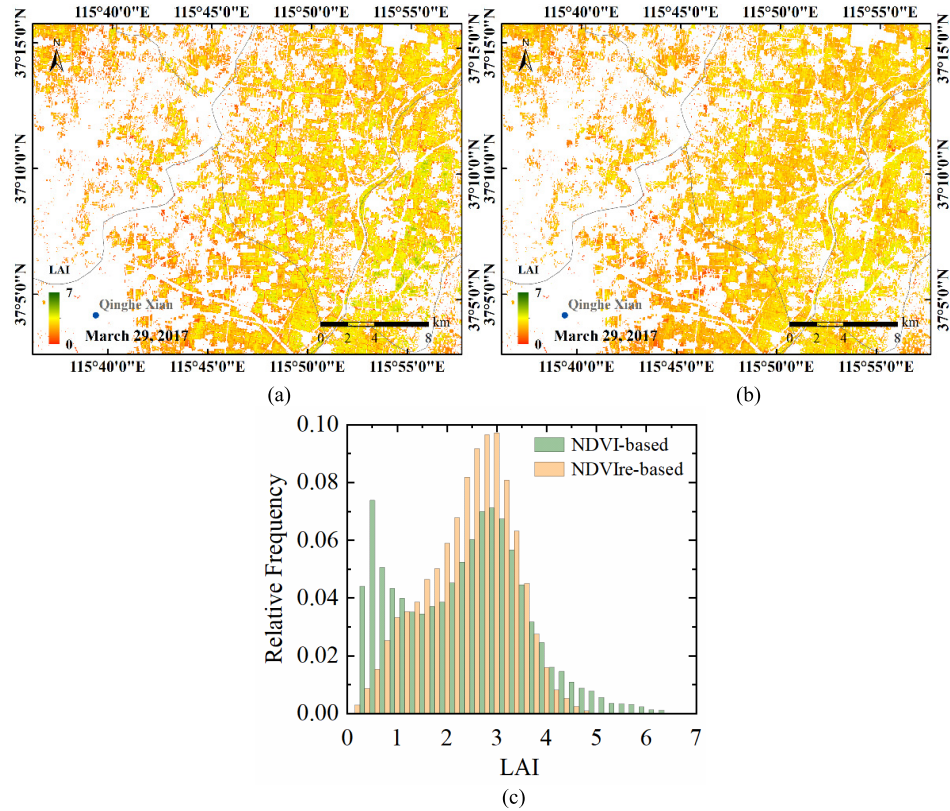


Fig. 10. Comparison of LAI images in HB on March 29, 2017, based on the (a) NDVI-based and (b) NDVIRE-based methods. (c) Histograms of LAI images

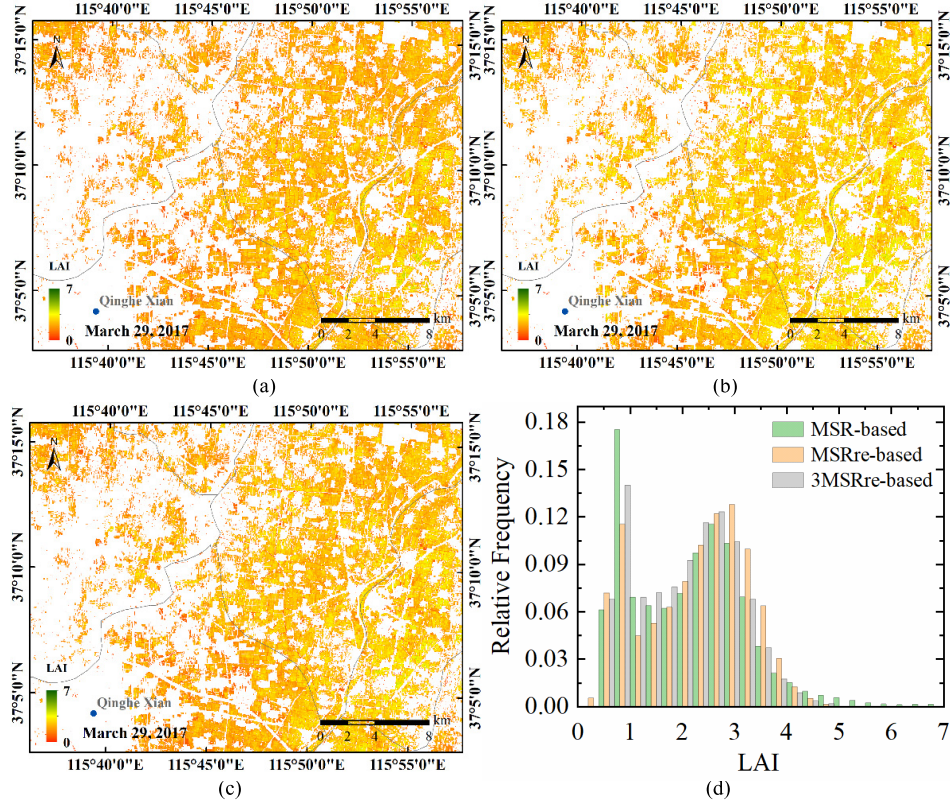


Fig. 11. Comparison of LAI images in HB on March 29, 2017, based on the (a) MSR-based, (b) MSRRE-based, and (c) 3MSRRE-based methods. (d) Histograms of LAI images

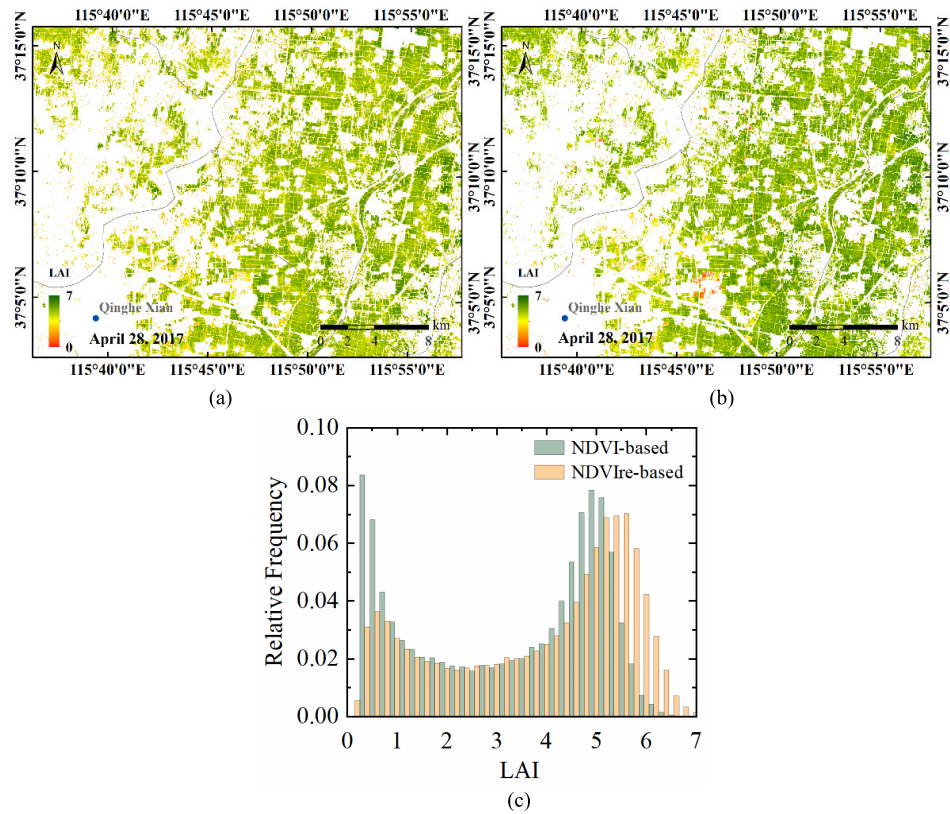


Fig. 12. Comparison of LAI images in HB on April 28, 2017, based on the (a) NDVI-based and (b) NDVIRE-based methods. (c) Histograms of LAI images

when LAI increases [1], [25]–[27]. The goal of this article was to investigate whether the greater red-edge band availability of Sentinel-2 could improve the quantification of LAI with vegetation index-based methods.

Although the red band is the most affected spectrum by chlorophyll because it is where the maximum absorption of chlorophyll occurs, it becomes saturated at high chlorophyll values, which results in a displacement in the red-edge domain. As a result, the reflectance of the RE1 band of Sentinel-2 is highly influenced by the chlorophyll content, whereas the red and RE2 bands are moderately influenced as mentioned in Section IV-A. This result is similar to the results of previous findings, which indicated that the influence of the chlorophyll content is constrained within 500–750 nm [71]. Thus it is possible to replace red with RE2 in the VIs to eliminate the effect of chlorophyll content on LAI retrieval and consequently improve the retrieval accuracy. However, the RE1 is not recommended to replace one of the original bands in the VIs for LAI retrieval because this band reflectance is mostly controlled by the chlorophyll content, and it could be used in combination with the existing VIs to increase information on canopy status.

The optimal bands for calculating NDVI, MSR, CI and WDRVI are RE2 and RE3 based on ground-measured LAI and Sentinel-2 data. The improvement in the LAI estimation accuracy with the utilization of these red-edge bands is remarkable for NDVI because it suffers from the greatest saturation problem at large LAI values. For different types of

crops, the values of the VIs of maize are slightly higher than those of wheat under the same LAI conditions in NDVI, MSR, CI and WDRVI, which are mainly derived from the spectral reflectance in the red and NIR bands of Sentinel-2 (Fig. 5 left column). However, this difference in LAI values for maize and wheat narrows or even disappears in the VIs involving RE2 and RE3 (Fig. 5 right column). Under the same LAI conditions the leaf chlorophyll content of maize is relatively higher than that of wheat [72]. Because the reflectance of red decreases while NIR remains almost unchanged as the chlorophyll content increases [71], the value of the VIs of maize is greater than that of wheat. The reflectances of RE2 and RE3 are less sensitive to the variations in chlorophyll content. Thus, the values of optimal red-edge VIs involved in RE2 and RE3 are insensitive to the type of crops. As a result, it is recommended that red-edge VIs with RE2 and RE3 should be utilized in the LAI estimation especially for a wide range of crops across multiple growth stages.

For the 3-band red-edge VIs the performance in LAI estimation is slightly improved compared to the performance of the 2-band red-edge VIs. This kind of improvement, generally ascribed to more spectral information from the red-edge domain, is introduced by a weighted coefficient. However, the added value of the additional red-edge band (especially RE1) for LAI estimation is also counteracted by the influence of the chlorophyll content, so the improvement in the accuracy of LAI estimation is not obvious for these 3-band red-edge VIs. The weighted parameter “*a*” may be diverse with

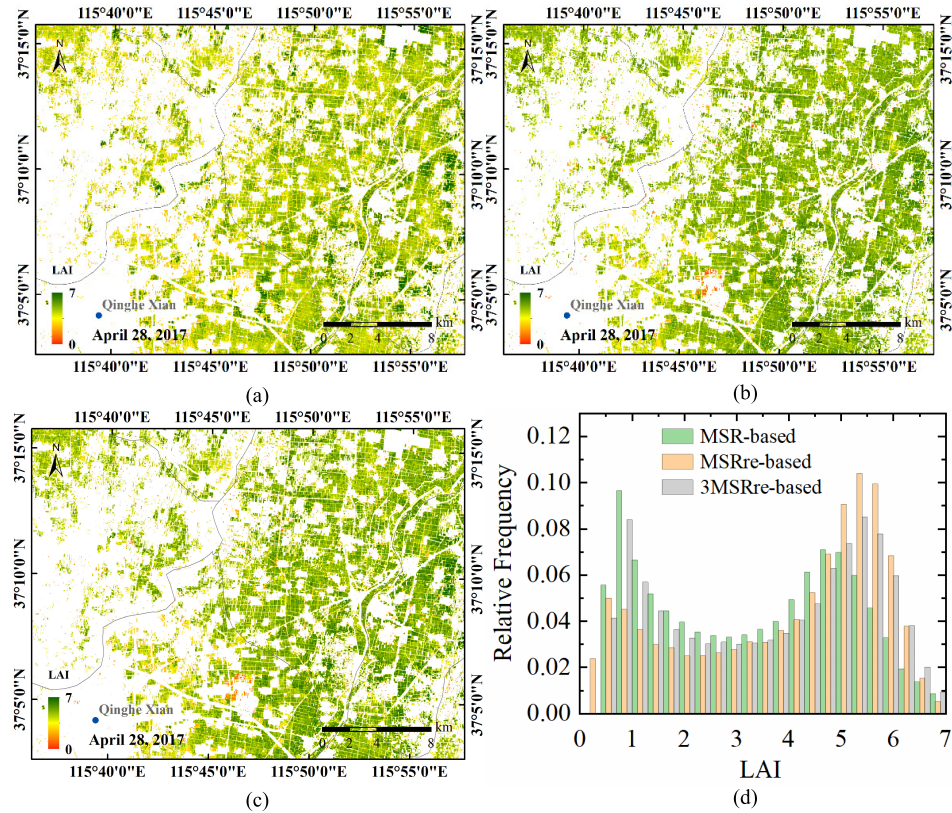


Fig. 13. Comparison of LAI images in HB on April 28, 2017, based on the (a) MSR-based, (b) MSRRe-based, and (c) 3MSRRe-based methods. (d) Histograms of LAI images

different LAI databases (e.g., different regions and different vegetation types). As a result, this parameter should be constantly updated before being applied.

Note that underestimation is still observed at $\text{LAI} > 5$ for the red-edge VIs (Fig. 8). One solution for addressing this problem is to segment the whole LAI range into several subranges and then estimate a regression equation (like Table VI) in each subrange, which may yield higher LAI estimation accuracy for large LAI values. A similar method has already been applied for maize and soybean LAI estimation based on NDVI and red-edge NDVI with an NDVI threshold setting of 0.7 [73]. Other factors (e.g., the leaf angle distribution, LAD) can also influence the canopy band reflectance and then affect the LAI retrieval accuracy. Maize canopies exhibit a planophile LAD while the wheat canopy presents a more erectophile LAD [18], [74]. The difference in LAD might also influence the values of the VIs derived from satellite data. However, these factors have less of an impact than LAI and chlorophyll content on canopy reflectance at the wavelengths we investigated [71], [75]. The leaf chlorophyll content changes intensely during different growth stages and its influence is our prime target to eliminate to improve the VIs for LAI estimation. Nevertheless, the relationships between LAI and VIs may be better if more factors are taken into consideration to reduce their impacts.

These 2-band and 3-band red-edge VIs are beneficial for crop growth monitoring with high spatial and temporal resolution in precision agriculture and have been applied in

HB wheat-cultivated regions. The estimated LAI shows more reasonable values than the NDVI-based results and reflects better seasonal characteristics of crops which further proves the credibility and reliability of our proposed red-edge VIs in LAI estimation. More work is still needed to validate these red-edge VIs over a broader range of crops and vegetation types, especially in dense canopies, and to determine a set of accurate and unified coefficients for LAI estimation in a wider agricultural system.

VI. CONCLUSION

This article investigates the possibility of using the three red-edge bands of Sentinel-2/MSI for LAI estimation based on VIs using ground-measured LAI data on wheat and maize over three sites in northern China. The sensitivity analysis results reveal that the first red-edge band (RE1, 705 nm) is affected by the influence of chlorophyll content the most followed by the second red-edge band (RE2, 740 nm), while the third red-edge band (RE3, 783 nm) is affected least. Taking four VIs NDVI, MSR, CI and WDRVI as examples, we found that the introduction of red-edge band reflectance can improve the LAI estimation accuracy especially for NDVI. For LAI retrievals from Sentinel-2 data, the optimal bands for calculating NDVI, MSR, CI and WDRVI are RE2 and RE3 rather than the conventional red and NIR bands. The LAI validation error is as low as 0.75. Compared to the existing NDVI calculated from the red and NIR reflectance, the effect of the saturation problem from the dense canopy (large LAI)

is reduced but still observable after incorporating the red-edge VIs. To improve the estimation for a large LAI canopy, a segmental estimation is also suggested for the red-edge VIs. Moreover, we proposed four 3-band red-edge VIs (3NDVI_{re}, 3MSR_{re}, 3CI_{re} and 3WDRV_{re}) for LAI estimation and the new VIs are found to work better than the 2-band method for sparse-to-moderate vegetated conditions. Finally, the red-edge VIs are applied in a wheat-cultivated area for LAI images retrieved on two dates (corresponding to two growth stages). Compared to the conventional NDVI-based method, the LAI estimated using the red-edge VIs is more reasonable especially in densely vegetated conditions and reflects better the seasonal characteristics of crops. Further research is needed to validate these VIs over a broader range of crops and to determine a set of accurate and unified coefficients for LAI estimation in precision agriculture.

ACKNOWLEDGMENT

The authors would like to thank the Sentinel Scientific Data Hub for providing Sentinel-2A MSI data and the software and algorithm for atmospheric correction.

REFERENCES

- [1] W. A. Dorigo, R. Zurita-Milla, A. J. W. de Wit, J. Brazile, R. Singh, and M. E. Schaepman, "A review on reflective remote sensing and data assimilation techniques for enhanced agroecosystem modeling," *Int. J. Appl. Earth Observ. Geoinf.*, vol. 9, no. 2, pp. 165–193, May 2007.
- [2] J. Verrelst *et al.*, "Optical remote sensing and the retrieval of terrestrial vegetation bio-geophysical properties—A review," *ISPRS J. Photogramm. Remote Sens.*, vol. 108, pp. 273–290, Oct. 2015.
- [3] R. B. Myneni *et al.*, "Global products of vegetation leaf area and fraction absorbed PAR from year one of MODIS data," *Remote Sens. Environ.*, vol. 83, pp. 214–231, Nov. 2002.
- [4] D. J. Watson, "Comparative physiological studies on the growth of field crops: I. Variation in net assimilation rate and leaf area between species and varieties, and within and between years," *Ann. Botany*, vol. 11, no. 41, pp. 41–76, 1947.
- [5] N. J. Bréda, "Ground-based measurements of leaf area index: A review of methods, instruments and current controversies," *J. Exp. Botany*, vol. 54, no. 392, pp. 2403–2417, Nov. 2003.
- [6] J. M. Chen and T. Black, "Defining leaf area index for non-flat leaves," *Plant, Cell Environ.*, vol. 15, no. 4, pp. 421–429, 1992.
- [7] K. Richter, C. Atzberger, F. Vuolo, P. Weih, and G. D'Urso, "Experimental assessment of the sentinel-2 band setting for RTM-based LAI retrieval of sugar beet and maize," *Can. J. Remote Sens.*, vol. 35, no. 3, pp. 230–247, Jun. 2009.
- [8] J. M. Chen, "Optically-based methods for measuring seasonal variation of leaf area index in boreal conifer stands," *Agricul. Forest Meteorol.*, vol. 80, nos. 2–4, pp. 135–163, Jul. 1996.
- [9] J. M. Chen, C. H. Menges, and S. G. Leblanc, "Global mapping of foliage clumping index using multi-angular satellite data," *Remote Sens. Environ.*, vol. 97, pp. 447–457, Sep. 2005.
- [10] Z. Xiao *et al.*, "Use of general regression neural networks for generating the GLASS leaf area index product from time-series MODIS surface reflectance," *IEEE Trans. Geosci. Remote Sens.*, vol. 52, no. 1, pp. 209–223, Jan. 2014.
- [11] I. Campos, L. Gonzalez-Gomez, J. Villodre, J. Gonzalez-Piqueras, A. E. Suyker, and A. Calera, "Remote sensing-based crop biomass with water or light-driven crop growth models in wheat commercial fields," *Field Crops Res.*, vol. 216, pp. 175–188, Feb. 2018.
- [12] J. Zhou, L. R. Khot, R. A. Boydston, P. N. Miklas, and L. Porter, "Low altitude remote sensing technologies for crop stress monitoring: A case study on spatial and temporal monitoring of irrigated pinto bean," *Precis. Agricult.*, vol. 19, no. 3, pp. 555–569, Jun. 2018.
- [13] J. Etchanchu *et al.*, "Effects of high spatial and temporal resolution Earth observations on simulated hydro meteorological variables in a cropland (southwestern France)," *Hydrol. Earth Syst. Sci.*, vol. 21, no. 11, p. 5693, 2017.
- [14] A. S. Milas, M. Romanko, P. Reil, T. Abeysinghe, and A. Marambe, "The importance of leaf area index in mapping chlorophyll content of corn under different agricultural treatments using UAV images," *Int. J. Remote Sens.*, vol. 39, nos. 15–16, pp. 5415–5431, Mar. 2018.
- [15] M. Battude *et al.*, "Estimating maize biomass and yield over large areas using high spatial and temporal resolution sentinel-2 like remote sensing data," *Remote Sens. Environ.*, vol. 184, pp. 668–681, Oct. 2016.
- [16] A. Chlingaryan, S. Sukkarieh, and B. Whelan, "Machine learning approaches for crop yield prediction and nitrogen status estimation in precision agriculture: A review," *Comput. Electron. Agricult.*, vol. 151, pp. 61–69, Aug. 2018.
- [17] V. Houlés, M. Guérif, and B. Mary, "Elaboration of a nitrogen nutrition indicator for winter wheat based on leaf area index and chlorophyll content for making nitrogen recommendations," *Eur. J. Agronomy*, vol. 27, no. 1, pp. 1–11, Jul. 2007.
- [18] A. Viña, A. A. Gitelson, A. L. Nguy-Robertson, and Y. Peng, "Comparison of different vegetation indices for the remote assessment of green leaf area index of crops," *Remote Sens. Environ.*, vol. 115, no. 12, pp. 3468–3478, Dec. 2011.
- [19] J. Liu, E. Pattey, and G. Jégo, "Assessment of vegetation indices for regional crop green LAI estimation from Landsat images over multiple growing seasons," *Remote Sens. Environ.*, vol. 123, pp. 347–358, Aug. 2012.
- [20] D. S. Kimes, Y. Knyazikhin, J. L. Privette, A. Abuelgasim, and F. Gao, "Inversion methods for physically-based models," *Remote Sens. Rev.*, vol. 18, nos. 2–4, pp. 381–439, 2000.
- [21] J. P. R. Caicedo, J. Verrelst, J. Muñoz-Marí, J. Moreno, and G. Camps-Valls, "Toward a semiautomatic machine learning retrieval of biophysical parameters," *IEEE J. Sel. Topics Appl. Earth Observ. Remote Sens.*, vol. 7, no. 4, pp. 1249–1259, Apr. 2014.
- [22] R. Houborg and M. F. McCabe, "A hybrid training approach for leaf area index estimation via Cubist and random forests machine-learning," *ISPRS J. Photogramm. Remote Sens.*, vol. 135, pp. 173–188, Jan. 2018.
- [23] J. Verrelst *et al.*, "Machine learning regression algorithms for biophysical parameter retrieval: Opportunities for sentinel-2 and -3," *Remote Sens. Environ.*, vol. 118, pp. 127–139, Mar. 2012.
- [24] J. W. Rouse, R. H. Haas, J. A. Schell, and D. W. Deering, "Monitoring vegetation systems in the great plains with ERTS," Texas A&M Univ., College Station, TX, USA, Tech. Rep. PAPER-A20, 1974.
- [25] O. Mutanga and A. K. Skidmore, "Narrow band vegetation indices overcome the saturation problem in biomass estimation," *Int. J. Remote Sens.*, vol. 25, no. 19, pp. 3999–4014, 2004.
- [26] S. Potithep, S. Nagai, K. N. Nasahara, H. Muraoka, and R. Suzuki, "Two separate periods of the LAI-VIs relationships using in situ measurements in a deciduous broadleaf forest," *Agricult. Forest Meteorol.*, vol. 169, pp. 148–155, Feb. 2013.
- [27] Y. Sun, H. Ren, T. Zhang, C. Zhang, and Q. Qin, "Crop leaf area index retrieval based on inverted difference vegetation index and NDVI," *IEEE Geosci. Remote Sens. Lett.*, vol. 15, no. 11, pp. 1662–1666, Nov. 2018.
- [28] J. M. Chen, "Evaluation of vegetation indices and a modified simple ratio for boreal applications," *Can. J. Remote Sens.*, vol. 22, no. 3, pp. 229–242, Jul. 1996.
- [29] A. A. Gitelson, "Wide dynamic range vegetation index for remote quantification of biophysical characteristics of vegetation," *J. Plant Physiol.*, vol. 161, no. 2, pp. 165–173, 2004.
- [30] R. Pu, P. Gong, G. S. Biging, and M. R. Larrieu, "Extraction of red edge optical parameters from hyperion data for estimation of forest leaf area index," *IEEE Trans. Geosci. Remote Sens.*, vol. 41, no. 4, pp. 916–921, Apr. 2003.
- [31] Q. Xie *et al.*, "Vegetation indices combining the red and red-edge spectral information for leaf area index retrieval," *IEEE J. Sel. Top. Appl. Earth Observ. Remote Sens.*, vol. 11, no. 5, pp. 1482–1493, May 2018.
- [32] Y. Zhu *et al.*, "Exploring the potential of worldview-2 red-edge band-based vegetation indices for estimation of mangrove leaf area index with machine learning algorithms," *Remote Sens.*, vol. 9, no. 10, p. 1060, Oct. 2017.
- [33] D. N. H. Horler, M. Dockray, and J. Barber, "The red edge of plant leaf reflectance," *Int. J. Remote Sens.*, vol. 4, no. 2, pp. 273–288, 1983.
- [34] J. Delegido, G. Fernández, S. Gandía, and J. Moreno, "Retrieval of chlorophyll content and LAI of crops using hyperspectral techniques: Application to PROBA/CHRIS data," *Int. J. Remote Sens.*, vol. 29, no. 24, pp. 7107–7127, Nov. 2008.
- [35] K.-S. Lee, W. B. Cohen, R. E. Kennedy, T. K. Maiersperger, and S. T. Gower, "Hyperspectral versus multispectral data for estimating leaf area index in four different biomes," *Remote Sens. Environ.*, vol. 91, nos. 3–4, pp. 508–520, Jun. 2004.

- [36] J. Delegido, J. Verrelst, C. M. Meza, J. P. Rivera, L. Alonso, and J. Moreno, "A red-edge spectral index for remote sensing estimation of green LAI over agroecosystems," *Eur. J.*, vol. 46, pp. 42–52, Apr. 2013.
- [37] A. Ramoelo, A. K. Skidmore, M. A. Cho, M. Schlerf, R. Mathieu, and I. M. A. Heitkönig, "Regional estimation of savanna grass nitrogen using the red-edge band of the spaceborne RapidEye sensor," *Int. J. Appl. Earth Observ. Geoinf.*, vol. 19, pp. 151–162, Oct. 2012.
- [38] O. Mutanga, E. Adam, and M. A. Cho, "High density biomass estimation for wetland vegetation using worldview-2 imagery and random forest regression algorithm," *Int. J. Appl. Earth Observ. Geoinf.*, vol. 18, pp. 399–406, Aug. 2012.
- [39] M. Drusch *et al.*, "Sentinel-2: ESA's optical high-resolution mission for GMES operational services," *Remote Sens. Environ.*, vol. 120, pp. 25–36, May 2012.
- [40] I. Herrmann, A. Pimstein, A. Karnieli, Y. Cohen, V. Alchanatis, and D. J. Bonfil, "LAI assessment of wheat and potato crops by VEN μ S and sentinel-2 bands," *Remote Sens. Environ.*, vol. 115, no. 8, pp. 2141–2151, Aug. 2011.
- [41] L. Korhonen, P. Packalen, and M. Rautiainen, "Comparison of sentinel-2 and landsat 8 in the estimation of boreal forest canopy cover and leaf area index," *Remote Sens. Environ.*, vol. 195, pp. 259–274, Jun. 2017.
- [42] J. Delegido, J. Verrelst, L. Alonso, and J. Moreno, "Evaluation of sentinel-2 red-edge bands for empirical estimation of green LAI and chlorophyll content," *Sensors*, vol. 11, no. 7, pp. 7063–7081, 2011.
- [43] M. Vincini, S. Amaducci, and E. Frazzi, "Empirical estimation of leaf chlorophyll density in winter wheat canopies using sentinel-2 spectral resolution," *IEEE Trans. Geosci. Remote Sens.*, vol. 52, no. 6, pp. 3220–3235, Jun. 2014.
- [44] J. A. A. Castillo, A. A. Apan, T. N. Maraseni, and S. G. Salmo III, "Estimation and mapping of above-ground biomass of mangrove forests and their replacement land uses in the Philippines using Sentinel imagery," *ISPRS J. Photogramm. Remote Sens.*, vol. 134, pp. 70–85, Dec. 2017.
- [45] J. G. P. W. Clevers, L. Kooistra, and M. M. van den Brande, "Using Sentinel-2 data for retrieving LAI and leaf and canopy chlorophyll content of a potato crop," *Remote Sens.*, vol. 9, no. 5, p. 405, Apr. 2017.
- [46] T. Majasalmi and M. Rautiainen, "The potential of Sentinel-2 data for estimating biophysical variables in a boreal forest: A simulation study," *Remote Sens. Lett.*, vol. 7, no. 5, pp. 427–436, Feb. 2016.
- [47] A. Pinar and P. J. Curran, "Technical note grass chlorophyll and the reflectance red edge," *Int. J. Remote Sens.*, vol. 17, no. 2, pp. 351–357, 1996.
- [48] A. A. Gitelson, A. Vina, V. Ciganda, D. C. Rundquist, and T. J. Arkebauer, "Remote estimation of canopy chlorophyll content in crops," *Geophys. Res. Lett.*, vol. 32, no. 8, Apr. 2005, Art. no. L08403.
- [49] A. A. Gitelson, Y. Gritz, and M. N. Merzlyak, "Relationships between leaf chlorophyll content and spectral reflectance and algorithms for non-destructive chlorophyll assessment in higher plant leaves," *J. Plant Physiol.*, vol. 160, no. 3, pp. 271–282, 2003.
- [50] T. Dong *et al.*, "Assessment of red-edge vegetation indices for crop leaf area index estimation," *Remote Sens. Environ.*, vol. 222, pp. 133–143, Mar. 2019.
- [51] F. Li *et al.*, "Improving estimation of summer maize nitrogen status with red edge-based spectral vegetation indices," *Field Crops Res.*, vol. 157, pp. 111–123, Feb. 2014.
- [52] M. Xu *et al.*, "Retrieving leaf chlorophyll content using a matrix-based vegetation index combination approach," *Remote Sens. Environ.*, vol. 224, pp. 60–73, Apr. 2019.
- [53] F. Vuolo *et al.*, "Data service platform for sentinel-2 surface reflectance and value-added products: System use and examples," *Remote Sens.*, vol. 8, no. 11, p. 938, Nov. 2016.
- [54] J.-B. Feret *et al.*, "PROSPECT-4 and 5: Advances in the leaf optical properties model separating photosynthetic pigments," *Remote Sens. Environ.*, vol. 112, no. 6, pp. 3030–3043, 2008.
- [55] S. Jacquemoud and F. Baret, "PROSPECT: A model of leaf optical properties spectra," *Remote Sens. Environ.*, vol. 34, no. 2, pp. 75–91, Nov. 1990.
- [56] W. Verhoef, "Light scattering by leaf layers with application to canopy reflectance modeling: The SAIL model," *Remote Sens. Environ.*, vol. 16, pp. 125–141, Oct. 1984.
- [57] W. Verhoef and H. Bach, "Coupled soil-leaf-canopy and atmosphere radiative transfer modeling to simulate hyperspectral multi-angular surface reflectance and TOA radiance data," *Remote Sens. Environ.*, vol. 109, no. 2, pp. 166–182, Jul. 2007.
- [58] K. Berger *et al.*, "Evaluation of the PROSAIL model capabilities for future hyperspectral model environments: A review study," *Remote Sens.*, vol. 10, no. 1, p. 85, Jan. 2018.
- [59] A. M. Baldridge, S. J. Hook, C. I. Grove, and G. Rivera, "The ASTER spectral library version 2.0," *Remote Sens. Environ.*, vol. 113, no. 4, pp. 711–715, 2009.
- [60] X. Zou *et al.*, "Retrieval of leaf chlorophyll content in field crops using narrow-band indices: Effects of leaf area index and leaf mean tilt angle," *Int. J. Remote Sens.*, vol. 36, no. 24, pp. 6031–6055, Dec. 2015.
- [61] A. Saltelli, "Sensitivity analysis: Could better methods be used?" *J. Geophys. Res. Atmos.*, vol. 104, no. D3, pp. 3789–3793, Feb. 1999.
- [62] H. Varella, M. Guérif, and S. Buis, "Global sensitivity analysis measures the quality of parameter estimation: The case of soil parameters and a crop model," *Environ. Model. Softw.*, vol. 25, no. 3, pp. 310–319, Mar. 2010.
- [63] A. Saltelli, S. Tarantola, and K. P.-S. Chan, "A quantitative model-independent method for global sensitivity analysis of model output," *Technometrics*, vol. 41, no. 1, pp. 39–56, 1999.
- [64] S. Jay, F. Maupas, R. Bendoula, and N. Gorretta, "Retrieving LAI, chlorophyll and nitrogen contents in sugar beet crops from multi-angular optical remote sensing: Comparison of vegetation indices and PROSAIL inversion for field phenotyping," *Field Crops Res.*, vol. 210, pp. 33–46, Aug. 2017.
- [65] A. Gitelson and M. N. Merzlyak, "Spectral reflectance changes associated with autumn senescence of *aesculus hippocastanum* L. and *Acer platanoides* L. Leaves. Spectral features and relation to chlorophyll estimation," *J. Plant Physiol.*, vol. 143, no. 3, pp. 286–292, Mar. 1994.
- [66] C. Wu, Z. Niu, Q. Tang, and W. Huang, "Estimating chlorophyll content from hyperspectral vegetation indices: Modeling and validation," *Agricul. Forest Meteorol.*, vol. 148, nos. 8–9, pp. 1230–1241, 2008.
- [67] Y. Peng and A. A. Gitelson, "Application of chlorophyll-related vegetation indices for remote estimation of maize productivity," *Agricul. Forest Meteorol.*, vol. 151, no. 9, pp. 1267–1276, 2011.
- [68] F. E. Fassnacht *et al.*, "Importance of sample size, data type and prediction method for remote sensing-based estimations of aboveground forest biomass," *Remote Sens. Environ.*, vol. 154, pp. 102–114, Nov. 2014.
- [69] F. Canisius, R. Fernandes, and J. Chen, "Comparison and evaluation of medium resolution imaging spectrometer leaf area index products across a range of land use," *Remote Sens. Environ.*, vol. 114, no. 5, pp. 950–960, May 2010.
- [70] D. P. Turner, W. B. Cohen, R. E. Kennedy, K. S. Fassnacht, and J. M. Briggs, "Relationships between leaf area index and landsat TM spectral vegetation indices across three temperate zone sites," *Remote Sens. Environ.*, vol. 70, no. 1, pp. 52–68, Oct. 1999.
- [71] J. Verrelst, J. P. Rivera, and J. Moreno, "ARTMO's global sensitivity analysis (GSA) toolbox to quantify driving variables of leaf and canopy radiative transfer models," *EARSeL EProc. Speical*, vol. 2015, no. 2, pp. 1–11, 2015.
- [72] M. C. Gonzalez-Sanpedro, T. Le Toan, J. Moreno, L. Kerfoot, and E. Rubio, "Seasonal variations of leaf area index of agricultural fields retrieved from Landsat data," *Remote Sens. Environ.*, vol. 112, no. 3, pp. 810–824, 2008.
- [73] A. Ngui-Robertson, A. Gitelson, Y. Peng, A. Viña, T. Arkebauer, and D. Rundquist, "Green leaf area index estimation in maize and soybean: Combining vegetation indices to achieve maximal sensitivity," *Agronomy J.*, vol. 104, no. 5, pp. 1336–1347, Sep. 2012.
- [74] R. Houborg and E. Boegh, "Mapping leaf chlorophyll and leaf area index using inverse and forward canopy reflectance modeling and SPOT reflectance data," *Remote Sens. Environ.*, vol. 112, no. 1, pp. 186–202, Jan. 2008.
- [75] F. Yang *et al.*, "Comparison of different methods for corn LAI estimation over northeastern China," *Int. J. Appl. Earth Observ. Geoinf.*, vol. 18, pp. 462–471, Aug. 2012.



Yuanheng Sun received the B.S. degree from East China Normal University, Shanghai, China, in 2015. He is currently pursuing the Ph.D. degree with the School of Earth and Space Sciences, Peking University, Beijing, China.

His research interests include the remote sensing of vegetation and its response to global climate change.



Qiming Qin received the B.S. degree in geography from Nanjing Normal University, Nanjing, China, in 1982, the M.S. degree in geophysics from Shaanxi Normal University, Xi'an, China, in 1987, and the Ph.D. degree in geophysics from Peking University, Beijing, China, in 1990.

He is currently a Professor with the Institute of Remote Sensing and Geographic Information System, School of Earth and Space Sciences, Peking University.

Dr. Qin is the Executive Director of the Environmental Remote Sensing Commission of the Geographical Society of China and the Director of the China Association for Geographic Information System, the Chinese Society for Geodesy, Photogrammetry and Cartography, the China Hi-Tech Industrialization Association, and the Chinese Association of Young Scientists and Technicians. He has served as an Evaluator of the Domestic GIS Software Evaluation Expert Team of the China Association for Geographic Information System in 1996 and a Lead Evaluator of the GIS Software Evaluation Committee of the Ministry of Science and Technology of China in 1995. He also serves as the Secretary General of the National Steering Committee for Geography Education in Universities and Colleges, China, and the Remote Sensing Application Consortium of Universities and Colleges, China.



Huazhong Ren received the Ph.D. degree from Beijing Normal University, Beijing, China, and the Université de Strasbourg, Strasbourg, France, in 2013.

Since 2016, he has been an Assistant Professor with the Institute of Remote Sensing and Geographic Information System, School of Earth and Space Sciences, Peking University, Beijing. His research interests include land surface temperature/emissivity estimate from thermal infrared remote sensing data.



Tianyuan Zhang received the B.S. degree in remote sensing science and technology from Beihang University, Beijing, China, in 2015. He is currently pursuing the Ph.D. degree in cartography and geography information system with Peking University, Beijing.

Since 2015, he has been with the Institute of Remote Sensing and Geographic Information System, School of Earth and Space Sciences, Peking University. His research interests include agricultural remote sensing.



Shanshan Chen received the B.S. degree from the Wuhan University of Technology, Wuhan, China, in 2015, and the M.S. degree from Capital Normal University, Beijing, China, in 2018. She is currently pursuing the Ph.D. degree with Peking University, Beijing.

Her research interests include urban remote sensing and thermal infrared remote sensing.